




# Compressed-Sensing-Aided Space-Time Frequency Index Modulation

Siyao Lu, Ibrahim A. Hemadeh , *Student Member, IEEE*, Mohammed El-Hajjar , *Senior Member, IEEE*, and Lajos Hanzo 

**Abstract**—In space-time shift keying (STSK), the information is conveyed by both the spatial and time dimensions, which can be used to strike a tradeoff between the diversity and multiplexing gains. On the other hand, orthogonal frequency-division multiplexing (OFDM) relying on index modulation (IM) conveys information not only by the conventional signal constellations as in classical OFDM, but also by the indices of the subcarriers. In this paper, we combine the benefits of STSK and IM in order to strike a flexible tradeoff between the throughput and bit-error performance by transmitting extra information bits in each subcarrier block, while increasing the diversity order. In order to further improve this tradeoff, as well as to decrease the complexity of the detector, compressed sensing is combined with the proposed STSK-aided IM system. We first present the maximum likelihood (ML) detection, which forms the best-case bound on the proposed system's performance. Then, we propose a pair of reduced-complexity detection algorithms capable of approaching the ML detector's performance. Furthermore, in order to attain a near capacity performance, we propose a soft-input soft-output decoder that is capable of exchanging soft information with a channel decoder through iterative decoding.

**Index Terms**—OFDM, MIMO, space-time shift keying (STSK), frequency index modulation, compressed sensing (CS), coordinate interleave (CI), frequency-selective fading, maximum likelihood detection, reduced-complexity detector, soft detection, channel coding.

## I. INTRODUCTION

SPACE-TIME shift keying (STSK) [1], [2] has been regarded as an advantageous multifunctional multiple-input multiple-output (MIMO) technique because of its flexibility in providing both multiplexing and transmit diversity gains. Compared to the conventional spatial modulation (SM) [3], [4] and space-shift keying (SSK) [5], STSK exhibits both transmit and receive diversity gains instead of only attaining receive diversity gain, as in SM and SSK. Namely, STSK spreads information to both the spatial and time dimensions, where the information

is mapped to the classic  $\mathcal{L}$ -PSK/QAM symbols and additional information is transmitted by activating one out of  $Q$  dispersion matrices (DM) [1], [2].

On the other hand, the distortion due to multipath fading is the main challenge in wideband fading channels [2], and often MultiCarrier (MC) modulation is used for mitigating this distortion, which effectively converts the dispersive wideband channels into a number of parallel narrowband flat-fading subchannels [6]. Orthogonal frequency-division multiplexing (OFDM) is the most widespread MC modulation technique, as a benefit of its robustness in wideband channels and its low-complexity implementation. OFDM has been combined with STSK in [6]–[10], where it was shown that OFDM-aided STSK is capable of mitigating the performance degradation of SC-STSK operating in wideband channels.

Index modulation (IM) [11], [12] is an emerging concept, in which extra information bits are mapped to the indices of multiple transmission resources [11], [13], such as the indices of antennas [13], [14], subcarriers [15] or time slots [13]. Spatial Modulation (SM) [3], [16] constitutes a promising MIMO technique, which transmits information bits mapped to the indices of the active transmit antennas, which corresponds to exploiting the spatial domain. By contrast, OFDM with IM (OFDM-IM) [12], [15], [17], [18] is a beneficial frequency-domain IM technique, which has been proposed as an alternative to classical OFDM, where the information is transmitted both by the quadrature amplitude modulation symbols as well as by the indices of the active subcarriers [15]. In OFDM-IM not all available subcarriers are activated. For example, activating one out of four subcarriers allows us to convey two extra information bits per subcarrier block. Ishikawa *et al.* [12] show that OFDM-IM improves the error performance at low values of signal-to-noise ratio (SNR) compared to the classical OFDM over frequency-selective fading channels. In order to further improve the spectral efficiency of OFDM modulated systems, a variable number of active subcarriers per OFDM subblock was applied in [17], where the frequency-domain IM is generalized and the problem of selecting the optimal number of active subcarriers for OFDM-IM is investigated. In [19], a subcarrier level block interleaving technique is invoked for OFDM-IM to improve the performance in the presence of uncorrelated subcarriers. Basar *et al.* [20] combined coordinate interleaving with OFDM-IM to achieve an additional diversity gain. Additionally, a transmit diversity scheme for OFDM-IM was proposed by J. Choi [21] to achieve the diversity gain for improving the

Manuscript received October 3, 2017; revised February 7, 2018; accepted March 19, 2018. Date of publication March 22, 2018; date of current version July 16, 2018. This work was supported by the European Research Council's Advanced Fellow Grant and the Royal Society's Wolfson Research Merit Award. The review of this paper was coordinated by Prof. Y. L. Guan. (*Corresponding author: Lajos Hanzo.*)

The authors are with the School of Electronics and Computer Science, University of Southampton, Southampton SO17 1BJ, U.K. (e-mail: sl18e14@ecs.soton.ac.uk; ibrahimhemadeh@gmail.com; meh@ecs.soton.ac.uk; lh@ecs.soton.ac.uk).

Color versions of one or more of the figures in this paper are available online at <http://ieeexplore.ieee.org>.

Digital Object Identifier 10.1109/TVT.2018.2818298

performance under a frequency-fading environment. The most recent study by Wen *et al.* [22] investigated OFDM relying on hybrid in-phase/quadrature-phase index modulation (OFDM-HIQ-IM), which allows transmission of more information bits for indexing in each subcarrier block and achieves better error performance than conventional OFDM-IM. Additionally, Mao *et al.* [23] proposed a dual-mode OFDM technique for enhancing the attainable throughput of the conventional OFDM-IM for achieving an improved error performance. Additionally, OFDM-IM is also combined with MIMO techniques in [24] and [25], which are proposed as promising energy-efficient 5G wireless communications systems. The recent studies in [13], [26] and [27] have explored IM in different dimensions, where an improved error performance has been obtained by increasing the number of dimensions applied.

In recent years, compressed sensing (CS) [28] has attracted considerable attention as a typical example to recover the sparse signal from a small set of linear measurements. CS has been applied to various wireless communication applications by exploiting the sparsity of the target signal vector, such as channel estimation [29], interference cancellation [30] and symbol detection [31]. CS is first applied to OFDM-IM by Zhang *et al.* [32], where the CS-aided OFDM-IM is demonstrated to be capable of achieving a higher spectral efficiency and better error performance than the conventional OFDM-IM scheme over wideband channels. In [33], Choi *et al.* provides useful tips and tricks for the design of CS-assisted wireless communication systems. In [34], the structured CS-aided low-complexity detector is proposed to improve detection performance.

Shannon in [35] predicted that reliable communication systems can be provided by incorporating redundancy into the transmitted information relying on channel coding. Then several channel coding techniques have been proposed since 1950s, such as the Hamming code [36], the Convolutional Codes (CC) [37], the turbo coding [38] as well as other channel coding techniques presented in [39]. In 1974, a decoding technique known as the Maximum A Posteriori (MAP) algorithm was advocated in order to attain the minimum bit error ratio (BER) for the CC [40]. Then, the concept of concatenated codes was proposed [41] and then the turbo principle was extended to both concatenated block codes and convolutional codes [42]. In [38], parallel concatenation of two Recursive Systematic Convolutional (RSC) codes was applied, where the soft-decision detector can iteratively exchange extrinsic information between the decoders for the sake of achieving near capacity performance.

Against this background, the novel contributions of this paper can be summarized as follows:

- Considering the advantages of OFDM-STSK, OFDM-IM and CS-based OFDM-IM over frequency-selective fading channels, we propose CS-aided OFDM-STSK relying on frequency index modulation, where coordinate interleaving (CI) [19]–[21] is invoked for achieving an additional diversity gain for improving the performance.
- First, ML detection is used for recovering the information bits, which forms the best-case bound on the system's performance. Compared to the classical OFDM-STSK relying

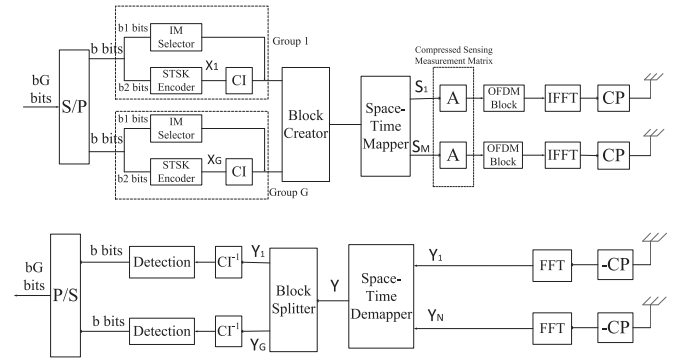


Fig. 1. The transceiver architecture.

on ML detection at the receiver, the proposed system exhibits about 8.1 dB SNR-gain at the BER of  $10^{-5}$  compared to that in the classical OFDM-STSK.

- Then, to mitigate the excessive complexity of the ML detector, we propose a pair of reduced-complexity detection algorithms, which attain a considerably lower complexity than the ML detector at the cost of a modest BER degradation.
- We also conceive SISO decoding for the proposed CS-aided OFDM-STSK-IM system. This is the first CS-aided OFDM-STSK-IM system relying on soft-decoding-aided channel coding in the open literature. Explicitly, a two-stage serially concatenated soft-decision detector is applied to the proposed CS-aided OFDM-STSK-IM system, where a pair of inner and outer decoders iteratively exchange their extrinsic information in order to achieve near capacity performance.

The rest of the paper is organized as follows. In Section II, the system model of CS-aided OFDM-STSK with frequency index modulation is introduced. Our performance analysis and simulation results are provided in Section III. Finally, our conclusions are provided in Section IV.

## II. SYSTEM MODEL

The block diagram of the proposed scheme is shown in Fig. 1, where  $bG$  number of information bits are divided into  $G$  parallel groups with  $b$  number of information bits processed in each group, as shown in Fig. 1. For each group of  $b$  bits,  $b_1$  bits are mapped to the IM selector, which chooses  $K$  active indices out of  $N_a$  available indices. The remaining  $b_2$  bits are used for generating  $K$  STSK codewords, and then these  $K$  codewords are coordinate-interleaved for providing an additional diversity gain to improve the BER performance. The  $K$  coordinate-interleaved codewords are then mapped to the active indices according to the IM selector, while the inactive indices are set to zero. Then the block creator collects all codewords from  $G$  groups in parallel and forms a frame, which is mapped to the spatial- and time-domain by the space-time mapper followed by OFDM modulation and then transmission.

In the system proposed in Fig. 1, we consider OFDM modulation with  $N_c$  subcarriers, which are equally divided into  $G$  subcarrier groups and each group contains  $M_g = N_c/G$

subcarriers in the frequency domain. In each subcarrier group,  $K$  number of indices are active out of  $N_a$  available subcarrier indices in the virtual domain. In OFDM,  $N_c$  may assume very large values, such as 128, 256, 512 or 1024 and if the index selector is applied directly to  $N_c$ , there could be a huge number of possible combinations for active indices, which makes the selection of active indices an almost impossible task. As a result, the subcarriers are partitioned into  $G$  smaller groups to perform index selection. As shown in Fig. 1, the information bits are divided into  $G$  groups at the input of the transmitter. The details of the transmitter and receiver models are discussed in the following sections.

#### A. Transmitter Model

As illustrated in Fig. 1,  $bG$  data bits are split into  $G$  groups of length  $b$  bits and then the corresponding  $b$  bits are processed in each group of the transmitter by the STSK encoder and the IM selector. The STSK encoder specified by the parameter  $(M, N, T, Q, L)$  is applied in our system, where  $M$  and  $N$  are the number of transmit and receive antennas, respectively,  $Q$  is the number of dispersion matrices and  $L$  represents the size of the constellation symbol. The STSK encoder generates space-time codewords from the information bits by activating a single dispersion matrix out of  $Q$  dispersion matrices and combined with the  $L$ -ary modulated symbols for transmission over  $T$  time slots. According to [2], each space-time codeword  $\mathbf{x} \in \mathbb{C}^{M \times T}$  that accommodates  $\log_2(QL)$  bits can be represented by

$$\mathbf{x} = x\mathbf{D}_q, \quad (1)$$

where  $\mathbf{D}_q \in \mathbb{C}^{M \times T}$  is the dispersion matrix selected from the matrix set  $\{\mathbf{D}_q\}_{q=1}^Q$  ( $q = 1, \dots, Q$ ), and  $x$  is a single  $L$ -PSK/QAM constellation symbol. As shown in Fig. 1,  $b_2$  data bits are processed by the STSK encoder in each group, where we have  $b_2 = K \times \log_2(QL)$ . In the  $g$ -th group, the STSK codewords are represented by  $\mathbf{X}_g[i]$ , where  $g = 1, 2, \dots, G$  and  $i = 1, 2, \dots, K$ .

In order to further increase the diversity gain and improve the system's performance, the CI technique of [20] is invoked for each group after the STSK encoder, as illustrated in Fig. 1. Specifically, CI is applied to the STSK codewords  $\mathbf{X}_g[i] \in \mathbb{C}^{M \times T}$  where  $i = 1, 2, \dots, K$  in the  $g$ -th group and  $K$  is an even number because the interleaving takes place between a pair of codewords. According to the CI, the real and imaginary parts of the complex data symbols are transmitted over different active indices of the system. The output signal after CI blocks is represented by  $\hat{\mathbf{X}}_g \in \mathbb{C}^{KM \times T}$  and contains  $K$  STSK codewords, which can be expressed as

$$\hat{\mathbf{X}}_g = \begin{bmatrix} \mathcal{R}\{\mathbf{X}_g[1]\} + j\mathcal{I}\{\mathbf{X}_g[2]\} \\ \mathcal{R}\{\mathbf{X}_g[2]\} + j\mathcal{I}\{\mathbf{X}_g[1]\} \\ \vdots \\ \mathcal{R}\{\mathbf{X}_g[K-1]\} + j\mathcal{I}\{\mathbf{X}_g[K]\} \\ \mathcal{R}\{\mathbf{X}_g[K]\} + j\mathcal{I}\{\mathbf{X}_g[K-1]\} \end{bmatrix}, \quad (2)$$

TABLE I  
A LOOKUP TABLE EXAMPLE FOR  $K = 2$  AND  $N_a = 4$

Bits	Indices	Blocks
[00]	{1, 2}	$[\mathbf{x}_1 \ \mathbf{x}_2 \ \mathbf{0} \ \mathbf{0}]$
[01]	{2, 3}	$[\mathbf{0} \ \mathbf{x}_1 \ \mathbf{x}_2 \ \mathbf{0}]$
[10]	{3, 4}	$[\mathbf{0} \ \mathbf{0} \ \mathbf{x}_1 \ \mathbf{x}_2]$
[11]	{1, 4}	$[\mathbf{x}_1 \ \mathbf{0} \ \mathbf{0} \ \mathbf{x}_2]$

where  $\mathcal{R}[\cdot]$  and  $\mathcal{I}[\cdot]$  represent the real and imaginary parts of the complex-valued symbol respectively, and the real part of the codeword after the CI block of Fig. 1 at the first active index comes from the real part of the first STSK codeword. By contrast, the imaginary part of the codeword after the CI block of Fig. 1 at the first active index comes from the imaginary part of the second STSK codeword and so on, for each of active indices.

The coordinate-interleaved space-time codewords  $\hat{\mathbf{X}}_g[i]$  in each subcarrier group are then mapped to  $K$  active subcarrier indices chosen from the  $N_a$  available indices according to the OFDM-IM principle [15], and each space-time matrix is applied to an active index. The remaining  $b_1 = \lfloor \log_2 C(N_a, K) \rfloor$  data bits in each group are used to select  $K$  out of  $N_a$  available indices by the IM selector, and only the selected active indices are allocated the space-time codewords.  $C(N_a, K)$  represents the number of possible combinations upon choosing  $K$  out of  $N_a$  and the notation  $\lfloor \cdot \rfloor$  represents the floor operation. The remaining  $(N_a - K)$  indices are inactive and set to zero. Additionally, the index selection procedure can be performed by referring to a look-up table [11], where the information bits are conveyed by the corresponding combinations of active indices. A look-up table example is provided in Table I for  $b_1 = 2$ ,  $K = 2$  and  $N_a = 4$ . For example, according to the look-up Table I, if the information bits of the IM selector are [00], the first and second indices out of the 4 available indices should be active indices, while the other two indices should be set to zero as shown in the table, and so on.

In the IM selector of Fig. 1, we consider a virtual domain rather than the frequency domain, where the number of the indices  $N_a$  available in the virtual domain is higher than the number of subcarriers  $M_g$  in the frequency domain of each group. With the aid of this virtual domain, the proposed system becomes capable of transmitting more information within the fixed bandwidth at no cost in terms of power. For example, there are  $N_c = 128$  subcarriers partitioned into  $G = 16$  subcarrier groups with  $M_g = 8$  subcarriers in each group and the STSK encoder specified by  $(2, 2, 2, 2, 2)$  is applied. For each group of the conventional OFDM-STSK-IM<sup>1</sup> having  $K = 2$  active subcarriers,  $b_2 = 2 \times \log_2(2 \times 2) = 4$  bits are used for encoding  $2^4 = 16$  STSK codewords and  $b_1 = \lfloor \log_2 C(8, 2) \rfloor = 4$  bits for selecting 2 active subcarriers out of 8 available subcarriers in each group, since we have  $2^4 = 16$  legitimate combinations. Hence a total of  $b = 8$  bits are transmitted through each

<sup>1</sup>The conventional OFDM-STSK-IM is the OFDM-IM technique without applying the CS.

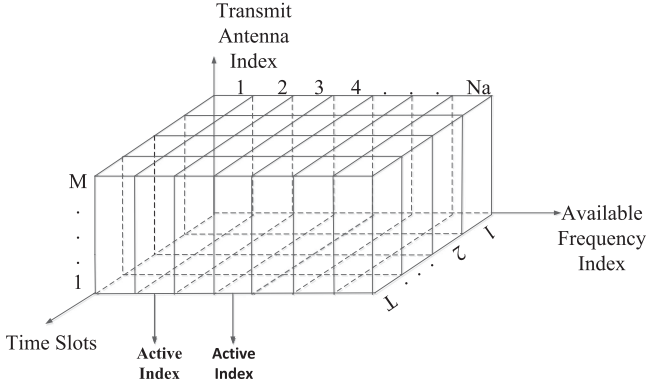


Fig. 2. The OFDM-STSK frame in the virtual domain for one subcarrier group with  $N_a$  available indices.

subcarrier group. By contrast, the proposed CS-aided OFDM-STSK-IM system introduces the virtual domain having  $N_a$  number of subcarriers for the IM selector, where the length of  $N_a$  in the virtual domain is designed much higher than that of  $M_g$  in the frequency domain. Explicitly,  $N_a = 15$  is assumed here, then  $b_1 = \lceil \log_2 C(15, 2) \rceil = 6$  bits are used for selecting  $2^6 = 64$  legitimate combinations relying on 2 active indices out of 15 available indices in the virtual domain. Quantitatively,  $b_2 = 2 \times \log_2(2 \times 2) = 4$  bits are used for the  $2^4 = 16$  STSK codewords of Fig. 1, yielding a total of  $b = 10$  bits transmitted through each subcarrier group. Hence, the proposed CS-aided system transmits more information than the conventional OFDM-STSK-IM scheme within the same bandwidth at no extra power consumption.”

After the allocation of active indices in each group, the symbols in the  $g$ -th group can be expressed as  $\bar{\mathbf{X}}_g = [x_g(1) x_g(2) \dots x_g(N_a)]$  in the virtual domain. The mapping of the STSK codewords to  $N_a$  parallel available indices is illustrated in Fig. 2 as a 3D structure, where the x-axis, y-axis and z-axis represent the time slots, the available frequency indices in the virtual domain and the transmit antennas, respectively. Additionally,  $N_a$  space-time matrices having  $(M \times T)$  elements are allocated in parallel slices. The slices which correspond to the active indices are set to the coordinate-interleaved space-time codewords and the other slices are set to zero.

The block creator of Fig. 1 concatenates  $G$  groups of codewords into a single frame and then the space-time symbols  $\bar{\mathbf{X}} = [\bar{\mathbf{X}}_0 \bar{\mathbf{X}}_1 \dots \bar{\mathbf{X}}_G]$  in the virtual domain are mapped to  $M$  transmit antennas over  $T$  time slots by the space-time mapper. With the aid of the space-time mapper of Fig. 1, we generate the transmit symbol vectors from  $M$  transmit antennas over  $T$  time slots, which can be written as  $[\mathbf{S}_1 \mathbf{S}_2 \dots \mathbf{S}_M]$  over one time slot, and the symbols at the  $m$ -th transmit antenna  $\mathbf{S}_m \in \mathbb{C}^{G N_a \times 1}$  can be also expressed as  $\mathbf{S}_m = [\mathbf{S}_m^1 \mathbf{S}_m^2 \dots \mathbf{S}_m^G]$ , where  $\mathbf{S}_m^g \in \mathbb{C}^{N_a \times 1}$  represents the symbols of the  $g$ -th group at the  $m$ -th transmit antenna.

In order to map the symbols in the virtual domain to the frequency domain for constructing the OFDM symbols, the measurement matrix  $\mathbf{A} \in \mathbb{C}^{M_g \times N_a}$  is applied to compress the  $N_a$ -dimensional signal  $\hat{\mathbf{S}}_m^g$  in the virtual domain into the  $M_g$ -

dimensional signal  $\hat{\mathbf{S}}_m^g$  in the frequency domain and this procedure is shown as

$$\hat{\mathbf{S}}_m^g = \mathbf{A} \mathbf{S}_m^g, \quad (3)$$

where  $\hat{\mathbf{S}}_m^g \in \mathbb{C}^{M_g \times 1}$  and (3) represents the classic mathematical model of CS [28]. However, there are no widely configured design principles for the CS measurement matrix  $\mathbf{A}$ . According to [28] and [33], the CS measurement matrix dominantly influences the receiver's symbol recovery performance. In order to make the recovery efficient, the columns of the matrix  $\mathbf{A}$  should be as uncorrelated as possible, so that the matrix preserves more energy of the input signal  $\mathbf{S}_m^g$ , where the mutual coherence of the measurement matrix  $\mathbf{A}$  is designed to be lower than  $1/(2K - 1)$ .

As illustrated in Fig. 1, the OFDM symbols in the frequency domain are obtained after the above procedures, and then the  $N_c$ -point inverse fast Fourier transform (IFFT) is applied to the frequency domain symbols at each transmit antenna, yielding the time-domain symbols  $[\bar{\mathbf{S}}_1 \bar{\mathbf{S}}_2 \dots \bar{\mathbf{S}}_M]$ . Finally, the cyclic prefix (CP) of length  $L_{cp}$ , which has to be longer than the channel's delay spread, is concatenated at the front of the time-domain symbols for eliminating the effects of the inter-symbol-interference over multipath fading channels. Then, the resultant signals are transmitted simultaneously from the  $M$  transmit antennas over the wireless channel.

### B. Detection of the Proposed System

The signal glanced from the transmit antennas is assumed to be transmitted over a  $L_{ch}$ -tap frequency-selective channel and the channel state information (CSI) is assumed to be perfectly known at the receiver.

Using the channel model  $h_{m,n}(n_c)$ , which represents the time-domain channel at the  $n_c$ -th subcarrier between the  $m$ -th transmit antenna as well as the  $n$ -th receive antenna and following the CP removal and FFT operation at the space-time demapper, the signal  $\mathbf{Y}[n_c] \in \mathbb{C}^{N \times T}$  received at the  $n_c$ -th subcarrier over  $N$  receive antennas can be expressed as

$$\mathbf{Y}[n_c] = \mathbf{H}[n_c] \hat{\mathbf{S}}[n_c] + \mathbf{n}[n_c], \quad (4)$$

where  $\mathbf{H}[n_c] \in \mathbb{C}^{N \times M}$  is the frequency-domain channel matrix at the  $n_c$ -th subcarrier,  $\hat{\mathbf{S}}[n_c] \in \mathbb{C}^{M \times T}$  is the compressed symbols at the  $n_c$ -th subcarrier transmitted from  $M$  transmit antennas over  $T$  time slots, and  $\mathbf{n}[n_c] \in \mathbb{C}^{N \times T}$  represents the additive white Gaussian noise (AWGN) following the distribution  $\mathcal{CN}(0, \delta_n^2)$ , where  $\delta_n^2$  represents the noise variance.

The received signal  $\mathbf{Y} \in \mathbb{C}^{N_c N \times T}$  in (4) is then passed through the block splitter and the received symbols in  $G$  groups are detected separately as shown in Fig. 1. Then the received signal  $\mathbf{Y}_g \in \mathbb{C}^{M_g N \times T}$  in the  $g$ -th group before detection can be obtained from (4), which is expressed further as:

$$\mathbf{Y}_g = \mathbf{H}_g \hat{\mathbf{A}} \mathbf{S}_g + \mathbf{n}_g, \quad (5)$$

where  $\mathbf{H}_g \in \mathbb{C}^{M_g N \times M_g M}$  represents the block-diagonal channel matrix of the whole  $g$ -th block,  $\hat{\mathbf{A}} \in \mathbb{C}^{M_g M \times N_a M}$  is the equivalent CS measurement matrix used for the signals glanced from the  $M$  transmit antennas, and  $\mathbf{S}_g \in \mathbb{C}^{N_a M \times T}$  contains the

information transmitted from the  $M$  transmit antennas over  $T$  time slots in the virtual domain. Additionally,  $\mathbf{n}_g \in \mathbb{C}^{M_g N \times T}$  is the AWGN matrix, which obeys the distribution  $\mathcal{CN}(0, \delta_n^2)$ .

For the analysis of different types of detectors, (5) can be expanded specifically for  $M_g$  consecutive subcarriers of block  $g$  as:

$$\begin{bmatrix} \mathbf{Y}_g^1 \\ \mathbf{Y}_g^2 \\ \vdots \\ \mathbf{Y}_g^{m_g} \\ \vdots \\ \mathbf{Y}_g^{M_g} \end{bmatrix} = \begin{bmatrix} \mathbf{H}_g^1 & \mathbf{0} & \dots & \mathbf{0} \\ \mathbf{0} & \mathbf{H}_g^2 & \dots & \mathbf{0} \\ \vdots & \vdots & \ddots & \vdots \\ \mathbf{0} & \mathbf{0} & \dots & \mathbf{H}_g^{M_g} \end{bmatrix} \begin{bmatrix} \hat{\mathbf{A}}_1 \\ \hat{\mathbf{A}}_2 \\ \vdots \\ \hat{\mathbf{A}}_{m_g} \\ \vdots \\ \hat{\mathbf{A}}_{M_g} \end{bmatrix} \mathbf{I}_g \hat{\mathbf{X}}_g + \mathbf{n}_g, \quad (6)$$

where  $\mathbf{Y}_g^{m_g} \in \mathbb{C}^{N \times T}$  represents the space-time codeword received at the  $m_g$ -th subcarrier in group  $g$ . Each channel matrix element  $\mathbf{H}_g^{m_g}$  has the size of  $(N \times M)$ , and the submatrix  $\hat{\mathbf{A}}_{m_g} \in \mathbb{C}^{M \times M N_a}$  in the equivalent CS measurement matrix is derived from the  $m_g$ -th row of the measurement matrix  $\mathbf{A}$  and can be specifically expanded as:

$$\hat{\mathbf{A}}_{m_g} = \begin{bmatrix} \mathbf{A}_{m_g} & \mathbf{0} & \dots & \mathbf{0} \\ \mathbf{0} & \mathbf{A}_{m_g} & \dots & \mathbf{0} \\ \vdots & \vdots & \ddots & \vdots \\ \mathbf{0} & \mathbf{0} & \dots & \mathbf{A}_{m_g} \end{bmatrix}, \quad (7)$$

where  $\mathbf{A}_{m_g}$  has the size of  $(1 \times N_a)$  and represents the  $m_g$ -th row-vector of the measurement matrix  $\mathbf{A}$ . In addition,  $\hat{\mathbf{X}}_g \in \mathbb{C}^{K M \times T}$  in (6) represents the coordinate-interleaved signal at the  $K$  active indices received from the  $M$  transmit antennas over  $T$  time slots in (2), and  $\mathbf{I}_g \in \mathbb{C}^{N_a M \times K M}$  is a block-diagonal matrix of the form

$$\mathbf{I}_g = \begin{bmatrix} \mathbf{I}_g^1 & \mathbf{0} & \dots & \mathbf{0} \\ \mathbf{0} & \mathbf{I}_g^2 & \dots & \mathbf{0} \\ \vdots & \vdots & \ddots & \vdots \\ \mathbf{0} & \mathbf{0} & \dots & \mathbf{I}_g^M \end{bmatrix}, \quad (8)$$

which illustrates the specific mapping pattern of selecting  $K$  active indices out of  $N_a$  available indices in the virtual domain for  $M$  transmit antennas. In (8) each submatrix  $\mathbf{I}_g^m \in \mathbb{C}^{N_a \times K}$  represents the index combination mapping pattern at the  $m$ -th transmit antenna, and the  $N_a$  rows in  $\mathbf{I}_g^m$  represent the  $N_a$  available frequency indices shown in Fig. 2, while the  $K$  columns in matrix  $\mathbf{I}_g^m$  represent the  $K$  selected active indices. Additionally, we assume that the index mapping pattern is the same for the  $M$  transmit antennas, where  $\mathbf{I}_g^1 = \mathbf{I}_g^2 = \dots = \mathbf{I}_g^M$  in (8). For example, let us assume that there are 2 transmit antennas, where the first and second indices are selected as active indices out of the 4 available indices in the virtual domain. Then the mapping

matrix for 2 transmit antennas is shown as:

$$\mathbf{I}_g = \begin{bmatrix} \mathbf{I}_g^1 & \mathbf{0} \\ \mathbf{0} & \mathbf{I}_g^2 \end{bmatrix} = \begin{bmatrix} 1 & 0 & \vdots & 0 & 0 \\ 0 & 1 & \vdots & 0 & 0 \\ 0 & 0 & \vdots & 0 & 0 \\ 0 & 0 & \vdots & 0 & 0 \\ \dots & \dots & \dots & \dots & \dots \\ 0 & 0 & \vdots & 1 & 0 \\ 0 & 0 & \vdots & 0 & 1 \\ 0 & 0 & \vdots & 0 & 0 \\ 0 & 0 & \vdots & 0 & 0 \end{bmatrix}. \quad (9)$$

In the following, we will first describe the ML detection followed by our proposed reduced-complexity algorithm conceived for reducing the excessive complexity of the ML detector without unduly eroding performance.

1) *Maximum Likelihood Detection*: In our proposed system model of (6), we should identify the matrix required for detecting the information bits used in the index selector of Fig. 1 and also to detect the information bits used for constructing the STSK codewords for all active indices.

Using the matrix given in (6), the ML detection of the proposed CS-aided OFDM-STSK-IM for each block  $g$  is performed in the detection block of Fig. 1, which is formulated as

$$\langle \hat{q}, \hat{l}, \hat{I}_c \rangle = \arg \min_{q, l, I_c} \left\| \mathbf{Y}_g - \mathbf{H}_g \hat{\mathbf{A}}_{I_c} \hat{\mathbf{X}}_{g, q, l} \right\|^2, \quad (10)$$

where  $I_c$  represents the index-combination library, which contains all possible index combinations in the transmitter look-up table and  $\hat{\mathbf{X}}_{g, q, l}$  represents the  $K$  coordinate-interleaved space-time codewords in the  $g$ -th group. The total decoding complexity order of the ML detection given in (10) for one subcarrier group is  $\mathcal{O}(N_{IM} (QL)^K)$ , which is considerably higher than that of classical OFDM-STSK, whose complexity order of one subcarrier group is  $\mathcal{O}(M_g QL)$ . Therefore, we employ a reduced-complexity detector in our system for reducing the complexity of the ML detection of (10).

2) *Reduced-Complexity Detection*: We propose a pair of reduced-complexity detection techniques, which strike a trade-off between the performance and the complexity as detailed below.

The initialization stages are the same for both reduced-complexity techniques described as follows:

- 1) During the first stage,  $G$  independent and successive minimum mean square error (MMSE) detections are performed relying on (5) using the following MMSE filtering

matrix:

$$\mathbf{W}_g = \left[ (\mathbf{H}_g)^H \mathbf{H}_g + \frac{1}{\rho} \mathbf{I}_{MM_g} \right]^{-1} (\mathbf{H}_g)^H, \quad (11)$$

where  $\rho$  is the average signal-to-noise ratio (SNR) per symbol and  $\mathbf{H}_g$  of (5), represents the equivalent channel matrix for the  $g$ -th group. Following the left-multiplication of  $\mathbf{Y}_g$  of (5) with the MMSE filtering matrix  $\mathbf{W}_g$  of (11), the MMSE detection is performed as

$$\hat{\mathbf{S}}_g = \mathbf{W}_g \mathbf{H}_g \hat{\mathbf{A}} \mathbf{S}_g + \mathbf{W}_g \mathbf{n}_g = \hat{\mathbf{A}} \mathbf{S}_g + \hat{\mathbf{n}}_g, \quad (12)$$

where  $\hat{\mathbf{S}}_g \in \mathbb{C}^{MM_g \times T}$  is the estimate of the transmitted CS-processed signal and  $\hat{\mathbf{n}}_g \in \mathbb{C}^{MM_g \times T}$  is the noise matrix after MMSE channel equalization.

- 2) Secondly, in order to get rough estimates of the space-time codewords in the virtual domain, the Hermitian transpose  $\hat{\mathbf{A}}^H$  of the equivalent measurement matrix  $\hat{\mathbf{A}}$  is multiplied by  $\hat{\mathbf{S}}_g$  in (12), which is shown as

$$\tilde{\mathbf{S}}_g = \hat{\mathbf{A}}^H \hat{\mathbf{A}} \mathbf{S}_g + \tilde{\mathbf{n}}_g, \quad (13)$$

where  $(\hat{\mathbf{A}}^H \hat{\mathbf{A}}) \in \mathbb{C}^{MN_a \times MN_a}$  is a square matrix and  $\tilde{\mathbf{n}}_g = \hat{\mathbf{A}}^H \hat{\mathbf{n}}_g$  is an AWGN noise matrix.

- 3) Then, the estimated signal  $\tilde{\mathbf{S}}_g \in \mathbb{C}^{MN_a \times T}$  of (13) is rearranged into  $N_a$  consecutive space-time codewords, which have the same structure as shown in Fig. 2 and the rearranged signal is represented by  $\bar{\mathbf{S}}_g = [\bar{\mathbf{S}}_g^1 \bar{\mathbf{S}}_g^2 \dots \bar{\mathbf{S}}_g^{N_a}]^T$ , where each  $\bar{\mathbf{S}}_g^{n_a} \in \mathbb{C}^{M \times T}$  is the estimated space-time codeword of the index  $n_a$  for group  $g$  in the OFDM-STSK frame shown in Fig. 2. Then the magnitudes of  $N_a$  consecutive space-time codewords obtained from  $\bar{\mathbf{S}}_g$  are calculated as  $[|\bar{\mathbf{S}}_g^1|^2 |\bar{\mathbf{S}}_g^2|^2 \dots |\bar{\mathbf{S}}_g^{N_a}|^2]$ . Because of the ‘sparsification’ of  $\mathbf{S}_g$  in (5), there are  $K$  nonzero codewords at the active indices shown in Fig. 2 complemented by  $(N_a - K)$  zero codewords at the inactive subcarrier indices. As a result, the  $N_a$  magnitudes provided should have  $K$  values, which are higher than the other  $(N_a - K)$  values<sup>2</sup>. After calculating and ordering the magnitudes, the specific subcarrier index having the highest magnitude may have a high probability to be one of the  $K$  active indices and the index with the lowest magnitude may have a high probability to be one of the  $(N_a - K)$  inactive indices.

Again, the above initialization procedures are the same for the two reduced-complexity techniques and in the following we explain how the two techniques operate, following the above initialization stages.

*a) Reduced-complexity detection Algorithm 1:* According to the calculated magnitudes at  $N_a$  consecutive subcarriers in the virtual domain, the subcarrier index having the highest magnitude among  $[|\bar{\mathbf{S}}_g^1|^2 |\bar{\mathbf{S}}_g^2|^2 \dots |\bar{\mathbf{S}}_g^{N_a}|^2]$  is selected by the detector as the first active subcarrier candidate<sup>3</sup>. Then ML detection is employed depending on the specific candidate selected. For example, if the first candidate  $n_a^1$  is selected, then ML detection is

performed for each block  $g$  which is formulated as

$$\langle \hat{q}, \hat{l}, \hat{I}_{n_a^1} \rangle = \arg \min_{q,l,I_{n_a^1}} \left\| \mathbf{Y}_g - \mathbf{H}_g \hat{\mathbf{A}}_{I_{n_a^1}} \hat{\mathbf{X}}_{g,q,l} \right\|^2, \quad (14)$$

where  $I_{n_a^1}$  represents a specific part of the index-combination library  $I_c$  in (10), which contains all possible index combinations with the index of the  $n_a^1$  candidate in the transmitter look-up table and  $\hat{\mathbf{X}}_{g,q,l}$  represents the coordinate-interleaved space-time codewords in the  $g$ -th group. Similarly, the subcarrier index  $n_a^2$  having the second highest magnitude is selected as the second candidate and ML detection is performed as

$$\langle \hat{q}, \hat{l}, \hat{I}_{n_a^2} \rangle = \arg \min_{q,l,I_{n_a^2}} \left\| \mathbf{Y}_g - \mathbf{H}_g \hat{\mathbf{A}}_{I_{n_a^2}} \hat{\mathbf{X}}_{g,q,l} \right\|^2, \quad (15)$$

where  $I_{n_a^2}$  contains all possible index combinations with the indices of  $n_a^1$  and  $n_a^2$  candidates in the transmitter look-up table, and so on for the rest of the selected candidates. Therefore, the detection with  $N_a$  candidates can exploit all possible index combinations in the transmitter look-up table and the performance merges with that of the ML detector of (10), whilst having the same complexity order.

Therefore, the complexity order of the reduced-complexity Algorithm 1 depends on the number  $\hat{N}_{IM}$  of index combinations processed from the look-up table provided at the transmitter, until the process is terminated. Then the generalised complexity order of Algorithm 1 is expressed as  $\mathcal{O}(\hat{N}_{IM} (QL)^K)$ . If all index candidates are selected at the detector, then we have  $\hat{N}_{IM} = N_{IM}$ , where  $N_{IM}$  represents the number of all index combinations provided by the transmitter and the complexity order of Algorithm 1 is exactly the same as that of ML detection. However, it is not necessary to process all index candidates to maintain the performance. Hence  $\hat{N}_{IM}$  is typically lower than the number of all possible combinations  $N_{IM}$ , where the complexity order  $\mathcal{O}(\hat{N}_{IM} (QL)^K)$  is lower than the complexity order  $\mathcal{O}(N_{IM} (QL)^K)$  of the ML detector.

*b) Reduced-complexity detection Algorithm 2:* With the benefit of CS, we propose an orthogonal matching pursuit (OMP)-like detection algorithm to make a locally optimal decision at each iteration, which is one of the most popular greedy algorithms [43].

- In the first iteration, the index having the highest magnitude among  $[|\bar{\mathbf{S}}_g^1|^2 |\bar{\mathbf{S}}_g^2|^2 \dots |\bar{\mathbf{S}}_g^{N_a}|^2]$  is selected as one candidate and represented by  $\hat{n}_a^1$ . With reference to the index combination table within the IM selector of the transmitter in Fig. 1, all combinations containing the selected index  $\hat{n}_a^1$  will be processed in the first iteration and  $C_1$  number of index combinations are assumed during the first iteration. Considering Table I as an example and assuming  $\hat{n}_a^1 = 1$ , the first index has the highest probability to be one of the 2 active indices and the combinations with the first index in Table I will be processed during the first iteration, where the index combinations  $\{1, 2\}$  and  $\{1, 4\}$  that both contain the first index are selected.
- Then in order to make our analysis comprehensive, the estimated signal  $\hat{\mathbf{S}}_g$  after channel equalization in (12) is expanded as

$$\hat{\mathbf{S}}_g = \hat{\mathbf{A}} \mathbf{I}_g \hat{\mathbf{X}}_g + \hat{\mathbf{n}}_g = \hat{\mathbf{A}}_g \hat{\mathbf{X}}_g + \hat{\mathbf{n}}_g, \quad (16)$$

<sup>2</sup>This is not true at very low SNRs, when the noise variance is high.

<sup>3</sup>The candidate in reduced-complexity techniques represents the subcarrier index which is selected according to the magnitudes calculated and ordered in the virtual domain.

where the matrix  $\mathbf{I}_g$  explained in (8) illustrates the specific index combination of selecting  $K$  active indices out of  $N_a$  available indices in the virtual domain for  $M$  transmit antennas. Additionally, according to the principle of the OMP algorithm, the process of  $\hat{\mathbf{A}}_g = \hat{\mathbf{A}}\mathbf{I}_g$  creates an over-determined scenario for the proposed detection system [43]. In this scenario, the simple least squares solution can be employed to recover the index combination used at the transmitter by using the pseudo-inverse operator. The pseudo-inverse operator  $\hat{\mathbf{A}}_g^+$  of  $\hat{\mathbf{A}}_g$  in (16) is denoted as

$$\hat{\mathbf{A}}_g^+ = \left( \hat{\mathbf{A}}_g^H \hat{\mathbf{A}}_g \right)^{-1} \hat{\mathbf{A}}_g^H, \quad (17)$$

which is multiplied with  $\hat{\mathbf{S}}_g$  in (16) and  $\hat{\mathbf{A}}_g^+ \hat{\mathbf{A}}_g = \mathbf{I}_{KM} + \mathbf{e}$  is obtained to recover the transmitted signal  $\hat{\mathbf{X}}_g$  in the  $g$ -th block, where  $\mathbf{e}$  is the error matrix owing to the mismatch of the index combinations. Hence the estimated signal  $\hat{\mathbf{X}}_g$  can be written in the general format of:

$$\hat{\mathbf{X}}_g = \hat{\mathbf{X}}_g + \mathbf{e} + \hat{\mathbf{n}}_g. \quad (18)$$

In the first iteration, there are  $C_1$  number of index combinations containing the selected index  $\hat{n}_a^1$ . Hence  $C_1$  pseudo-inverse operators are generated and multiplied with  $\hat{\mathbf{S}}_g$  in (16).

- After obtaining the estimated codewords  $\hat{\mathbf{X}}_g$  in (18) at the  $K$  active indices in group  $g$ , the ML detection is applied to (18) for detecting the STSK codewords, index-by-index as follows:

$$\hat{x}_g(k, \hat{q}, \hat{l}) = \arg \min_{q, l} \left\| \hat{\mathbf{X}}_g(k) - x(q, l) \right\|^2, \quad (19)$$

where  $q$  and  $l$  are the dispersion matrix index and the symbol constellation index, respectively. Furthermore,  $\hat{q}$  and  $\hat{l}$  are the corresponding estimated indices, and  $\hat{x}_g(k, \hat{q}, \hat{l})$  represents the estimated STSK codeword associated with  $\hat{q}$  dispersion matrices and a constellation size of  $\hat{l}$  at the  $k$ -th active index,  $k = 1, 2, \dots, K$ .

- In the above stages of the first iteration, we can obtain  $C_1$  estimated signal matrices, where each matrix contains  $K$  space-time codewords over  $T$  time slots. In order to optimize the  $C_1$  estimated results in the first iteration, the best fit result can be found by evaluating  $\langle \arg \min \|\hat{\mathbf{S}}_g - \hat{\mathbf{I}}_g^1 \hat{\mathbf{x}}_g^{c_1}\|^2 \rangle$  to get the specific index mapping matrix and the STSK codeword, which can minimize the difference between the received signal and the estimated signal, where  $c_1 = 1, 2, \dots, C_1$ , and  $\hat{\mathbf{I}}_g^{c_1}$  is the mapping matrix for the  $c_1$ -th processed index combination in the first iteration and  $\hat{\mathbf{x}}_g^{c_1}$  illustrates the estimated coordinate-interleaved space-time codewords at the  $K$  active indices over  $T$  time slots in group  $g$  for the  $c_1$ -th processed index combination in the iteration considered. Then the optimized result  $\hat{\mathbf{S}}_g^1$  obtained during the first iteration contains the information of the best-fit index selection pattern. Finally, the information bits detected for constructing space-time codewords are obtained.

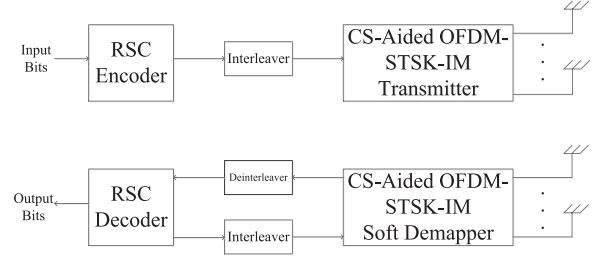


Fig. 3. The transceiver structure of the soft-decision system.

The signals  $[\hat{\mathbf{S}}_g^1 \hat{\mathbf{S}}_g^2 \hat{\mathbf{S}}_g^3 \dots]$  optimized for all iterations can be obtained by repeating the above stages for the rest of the iterations.

In fact, it is unnecessary to invoke all iterations as a benefit of applying the pseudo-inverse shown in (18), since the potential error matrix  $\mathbf{e}$  in (18) becomes  $\mathbf{0}$  if the correct index combination is detected. As a result, an error threshold  $e_{th}$  can be set up to terminate the process of iterations for reducing the computational complexity. The potential residual error  $e_g^i$  after the  $i$ -th iteration becomes:

$$e_g^i = \left\| \mathbf{Y}_g - \mathbf{H}_g \hat{\mathbf{A}} \hat{\mathbf{S}}_g^i \right\|^2. \quad (20)$$

If the error  $e_g^i$  in the  $i$ -th iteration is lower than or equal to the threshold error  $e_{th}$ , then the process can be terminated and the correct index modulation bits and STSK information bits can be detected in the  $g$ -th group.

The complexity order of the reduced-complexity detection Algorithm 2 depends on the number of index combinations  $\tilde{N}_{IM}$  processed from the look-up table provided at the transmitter, until the process is terminated. Then the generalised complexity order of Algorithm 2 is expressed as  $\mathcal{O}(\tilde{N}_{IM} Q L K)$ , where  $\tilde{N}_{IM}$  is typically lower than the number of all possible combinations  $N_{IM}$ . Additionally, the maximum complexity order of Algorithm 2 is  $\mathcal{O}(N_{IM} Q L K)$ , which is still lower than the complexity order  $\mathcal{O}(N_{IM} (Q L)^K)$  of the ML detector. Compared to the generalised complexity order  $\mathcal{O}(\hat{N}_{IM} (Q L)^K)$  of Algorithm 1 having  $\hat{N}_{IM} = \tilde{N}_{IM}$ , the complexity order of Algorithm 2 is lower than that of the first algorithm.

3) *Soft-Decision Detection*: In this section, we extend the proposed hard-decision receiver to soft-decision detection. The block diagram of a channel-coded system employing iterative detection at the receiver is shown in Fig. 3. The channel encoder encodes the information bits with the aid of a Recursive Systematic Convolutional (RSC) code to generate a bit stream, which is interleaved by the interleaver in Fig. 3 [44]. The interleaved bits are then modulated by the transmitter of the proposed system in Fig. 1 followed by transmission over the wireless channel.

As shown in Fig. 3, the two-stage soft-input soft-output (SISO) decoder is employed for iteratively exchanging soft extrinsic information in the form of Log Likelihood Ratios (LLRs) between the CS-aided OFDM-STSK-IM soft decoder and the RSC decoder [1]. Specifically, during each inner-outer decoding iteration<sup>4</sup>, the output LLRs of the soft decoder shown

<sup>4</sup>To avoid confusion with the iteration in the Reduced-Complexity Algorithm 2, we will refer to this as inner-outer iteration and we use the abbreviation IO-Iter.

in Fig. 3 are deinterleaved by the deinterleaver to produce the soft information fed into the RSC decoder as *a priori* LLRs. Having obtained the *a priori* LLRs as soft input, the RSC decoder then generates the extrinsic LLRs by invoking the Logarithmic Maximum a posteriori (Log-MAP) algorithm [45], where the extrinsic LLRs are interleaved and fed back to the CS-aided OFDM-STSK-IM soft decoder as *a priori* LLRs.

According to the conditional probability of the soft demapper of STSK systems in [1], the conditional probability  $p(\mathbf{Y}_g|\hat{\mathbf{S}}_g)$  of the received signal block  $\mathbf{Y}_g$  obtained from the equivalent system model represented in (5) can be expressed as:

$$\begin{aligned} p(\mathbf{Y}_g|\hat{\mathbf{S}}_g) &= \frac{1}{(\pi N_0)^{NT}} \exp\left(-\frac{\|\mathbf{Y}_g - \mathbf{H}_g \hat{\mathbf{A}}_g \hat{\mathbf{X}}_g\|^2}{N_0}\right) \\ &= \frac{1}{(\pi N_0)^{NT}} \exp\left(-\frac{\|\mathbf{Y}_g - \mathbf{H}_g \hat{\mathbf{S}}_g\|^2}{N_0}\right), \end{aligned} \quad (21)$$

where  $\hat{\mathbf{X}}_g$  represents the  $K$  number of coordinate interleaved space-time codewords in the  $g$ -th block and  $\hat{\mathbf{S}}_g$  denotes the compressed symbols in the  $g$ -th block. The received signal block  $\mathbf{Y}_g$  carries  $B$  channel-coded bits in the  $g$ -th block for both the index selector and the STSK encoder illustrated in Fig. 1. The channel-coded bit sequence in the  $g$ -th block can be represented as  $\mathbf{b} = [b_1, b_2, \dots, b_B]$  and the resultant extrinsic LLR value of bit  $b_i$ ,  $i = 1, \dots, B$ , can be expressed in (22), shown at the bottom of the page.  $(\hat{S}_g)_0^i$  and  $(\hat{S}_g)_1^i$  in (22) represent the sub-set of the space-time-frequency codewords, satisfying  $(\hat{S}_g)_0^i \equiv \{\hat{\mathbf{S}}_g \in \hat{S} : b_i = 0\}$  and  $(\hat{S}_g)_1^i \equiv \{\hat{\mathbf{S}}_g \in \hat{S} : b_i = 1\}$ , respectively. Furthermore,  $L_a(\cdot)$  in (22) represents the *a priori* LLR as the feedback from the RSC decoder to the soft decoder of the proposed system. In order to avoid numerical overflow and to simplify the soft-detection, the Jacobian logarithm of [46] is employed for computing (22) as

$$\begin{aligned} L_e(b_i) &= \text{jac}_{\hat{\mathbf{S}}_g \in (\hat{S}_g)_1^i} \left( -\frac{\|\mathbf{Y}_g - \mathbf{H}_g \hat{\mathbf{S}}_g\|^2}{N_0} + \sum_{j \neq i} b_j L_a(b_j) \right) \\ &\quad - \text{jac}_{\hat{\mathbf{S}}_g \in (\hat{S}_g)_0^i} \left( -\frac{\|\mathbf{Y}_g - \mathbf{H}_g \hat{\mathbf{S}}_g\|^2}{N_0} + \sum_{j \neq i} b_j L_a(b_j) \right). \end{aligned} \quad (23)$$

TABLE II  
THE TABLE FOR SYSTEM PARAMETERS IN SIMULATIONS

Parameters	Values
Multi-carrier System	OFDM
Number of subcarriers	128
Length of Cyclic Prefix	16
Number of subcarrier groups, $G$	16
Number of subcarriers/group, $M_g$	8
Number of available indices/group, $N_a$	16
Number of active indices/group, $K$	2 (or 4)
Channel Specification	COST2017-TU12 Rayleigh Fading

### III. SIMULATION RESULTS

In this section, the performance of the proposed CS-aided Space-Time Frequency IM system considered for transmission over frequency-selective fading channels is characterized. The system parameters used in our simulations are shown in Table II. In all simulations, we assume perfect channel state information (CSI) knowledge at the receiver. The comparisons between the classical OFDM-STSK, conventional OFDM-STSK-IM, and the CS-aided OFDM-STSK-IM are presented at the same transmission data rates. The BER performances of these schemes are evaluated by Monte Carlo simulations.

In Fig. 4, we compare the BER performance of the classical OFDM-STSK, conventional OFDM-STSK-IM, and the proposed CS-aided OFDM-STSK-IM schemes, where all these systems use ML detection and have the same transmission rate of 1.1111 bits/s/Hz for the sake of fair comparison (the transmission rate is calculated by  $\frac{bG}{(N_c + L_{cp})}$  bits/s/Hz). In order to keep the same transmission data rate, the three schemes apply the STSK encoders specified as STSK (2, 2, 2, 2, 2), STSK (2, 2, 2, 4, 2), and STSK (2, 2, 2, 2, 2), respectively, which contains 2 bits, 3 bits, and 2 bits per space-time codeword separately and each subcarrier group can transmit 10 data bits from 2 transmit antennas over 2 time slots across 8 subcarriers. Additionally, only 80 out of 128 subcarriers are applied by the classical OFDM-STSK scheme for keeping the same transmission rate of 1.1111 bits/s/Hz. As seen from Fig. 4, at a BER value of  $10^{-5}$ , the conventional OFDM-STSK-IM scheme operating without CS requires about 1.25 dB lower SNR than the classical OFDM-STSK system, and the proposed CS-aided system achieves approximately 7.92 dB and 6.67 dB lower SNR than the classical OFDM-STSK system and the conventional OFDM-STSK-IM system, respectively. We can

$$\begin{aligned} L_e(b_i) &= \ln \frac{\sum_{\hat{\mathbf{S}}_g \in (\hat{S}_g)_1^i} p(\mathbf{Y}_g|\hat{\mathbf{S}}_g) \exp\left[\sum_{j \neq i} b_j L_a(b_j)\right]}{\sum_{\hat{\mathbf{S}}_g \in (\hat{S}_g)_0^i} p(\mathbf{Y}_g|\hat{\mathbf{S}}_g) \exp\left[\sum_{j \neq i} b_j L_a(b_j)\right]} \\ &= \ln \frac{\sum_{\hat{\mathbf{S}}_g \in (\hat{S}_g)_1^i} \exp\left[-\frac{\|\mathbf{Y}_g - \mathbf{H}_g \hat{\mathbf{S}}_g\|^2}{N_0} + \sum_{j \neq i} b_j L_a(b_j)\right]}{\sum_{\hat{\mathbf{S}}_g \in (\hat{S}_g)_0^i} \exp\left[-\frac{\|\mathbf{Y}_g - \mathbf{H}_g \hat{\mathbf{S}}_g\|^2}{N_0} + \sum_{j \neq i} b_j L_a(b_j)\right]} \end{aligned} \quad (22)$$



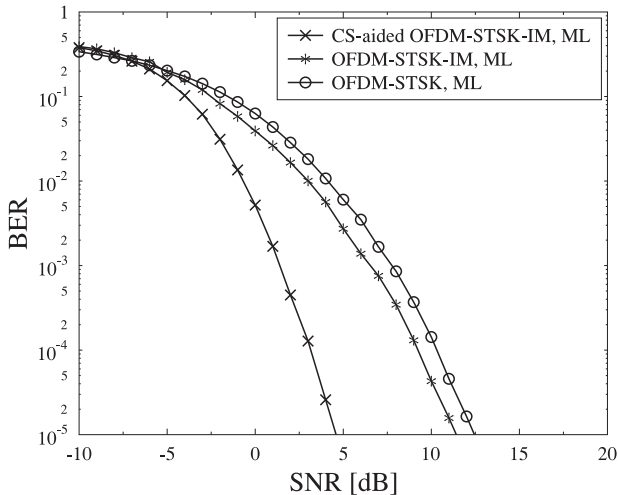


Fig. 4. BER performances of classical OFDM-STSK, conventional OFDM-STSK-IM, and CS-aided OFDM-STSK-IM by employing ML detection with the same transmission rate of 1.1111 bits/s/Hz.

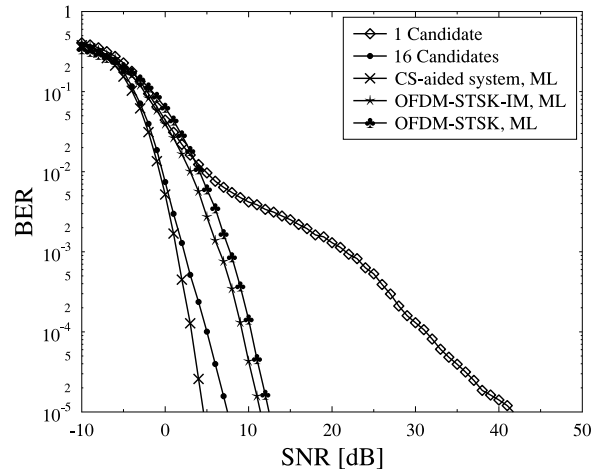


Fig. 6. BER performances of all schemes applying both ML detection and the reduced-complexity detection Algorithm 2 with the same transmission rate of 1.1111 bits/s/Hz.

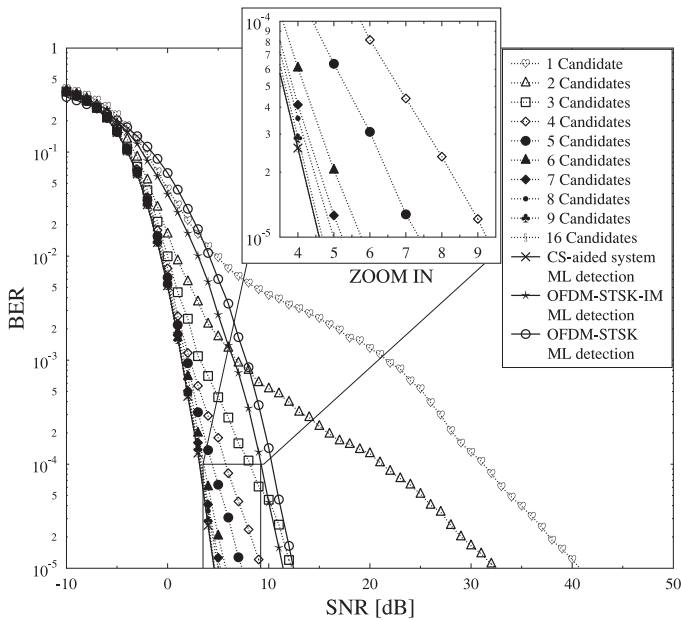


Fig. 5. BER performances of all schemes applying both ML detection and the reduced-complexity detection Algorithm 1 with the same transmission rate of 1.1111 bits/s/Hz.

observe that the proposed CS-aided system significantly outperforms both the classical OFDM-STSK and the conventional OFDM-STSK-IM. When considering these three systems characterized in Fig. 4, the complexity order of the proposed CS-aided system is  $\mathcal{O}(64 \times (2 \times 2)^2) = \mathcal{O}(1024)$ , which is the same as the complexity order of  $\mathcal{O}(16 \times (2 \times 4)^2) = \mathcal{O}(1024)$  of the conventional OFDM-STSK-IM system, while the complexity order of the classical OFDM-STSK scheme is  $\mathcal{O}(8 \times (2 \times 2)) = \mathcal{O}(32)$ . Because of the considerably higher complexity of the proposed system, the proposed reduced-complexity detectors are applied in the simulation results shown in Figs. 5 and 6.

In Fig. 5, we apply the proposed reduced-complexity detection Algorithm 1 to the CS-aided scheme and compare the

BER performance attained to that of the CS-aided scheme using ML detection, as shown in Fig. 4. We have portrayed the BER performances of the CS-aided OFDM-STSK-IM system employing the reduced-complexity detector using 1 to 16 number of candidates, as well as the other two schemes shown in Fig. 4. For the sake of fair comparison, again, all figures have the same transmission rate of 1.1111 bits/s/Hz, the same bandwidth and use CI to increase the diversity gain. The reduced-complexity detector characterized in Fig. 5 is capable of achieving a considerably lower complexity while choosing adequate number of candidates than the same system using the ML detector. According to the simulation results of the schemes exploiting different number of candidates in Fig. 5, the systems using 1 candidate, 2 candidates and 3 candidates have worse performances than these of the three schemes shown in Fig. 4. We can observe from Fig. 5 that the system using 4 candidates achieves about 2 dB better performance than that of the conventional IM system at a BER of  $10^{-5}$ , while the system with 5 candidates can achieve about 1.95 dB better performance than the system using 4 candidates, as well as the system with 6 candidates achieves about 1.55 dB better performance than using 5 candidates. Then it is shown in Fig. 5 that the systems exploiting over 7 candidates in the reduced-complexity system has performance that approaches the performance of the ML detection. In addition, the detector using 16 candidates attains identical performance as the ML detector, as well as the complexity order. Hence, in the case of Fig. 5, using 4 to 5 candidates is enough to maintain a better performance than that of the classical OFDM-STSK-IM system shown in Fig. 5 with considerably lower complexity.

In order to further reduce the complexity of the detector, the reduced-complexity detection Algorithm 2 is proposed and simulation results under the same transmission data rate of 1.1111 bits/s/Hz are shown in Fig. 6. Again, the three schemes applying the ML detection in Fig. 4 are also shown in Fig. 6 for sake of convenient comparison. In Fig. 6, only performances of Algorithm 2 with 1 candidate and 16 candidates are illustrated in the figure. The system applying only one candidate has the worst performance and the system applying 16 candidates which

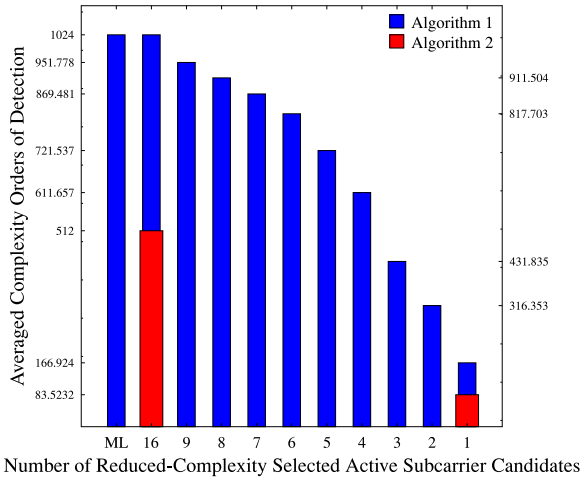


Fig. 7. Averaged complexity orders with different number of reduced-complexity selected active subcarrier candidates applied for both Algorithms 1 and 2.

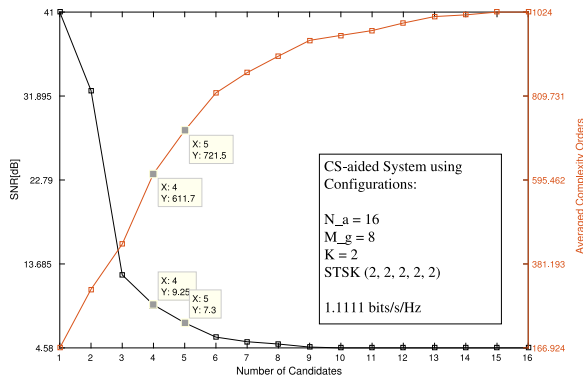


Fig. 8. The required SNR and averaged complexity orders required to attain a BER value of  $10^{-5}$  for the proposed CS-aided OFDM-STSK-IM decoding Algorithm 1.

can exploit all possible subcarrier index combinations from the look-up table of the transmitter has the best performance of the proposed reduced-complexity detection Algorithm 2. The best case of the Algorithm 2 achieves about 2.6 dB worse performance than that of the ML detection, while the complexity order  $O(512)$  of the best case is considerably lower than that of the ML detection which is  $O(1024)$ . Hence, there is a trade-off between the complexity and the BER performance while selecting schemes.

Furthermore, Fig. 7 illustrates the detection complexity imposed by detecting each group of symbols, when both the ML and the proposed pair of reduced-complexity detectors are employed. Here, the averaged complexity orders in Fig 7 are obtained by simulations and can fully illustrate the detection complexity of the proposed reduced-complexity schemes shown in Figs. 5 and 6. In Fig. 7, the reduced-complexity detector 1 employing  $I_n = 1, \dots, 9$  and  $N_a$  candidates is considered for the proposed scheme. It can be readily shown in Fig. 7 that the detection complexity of the proposed reduced-complexity detector 1 can be significantly reduced depending on the number of candidates exploited in the proposed system, especially when the number of candidates is set to under 5 candidates. Considering both the BER performance in Fig. 5 and the detection

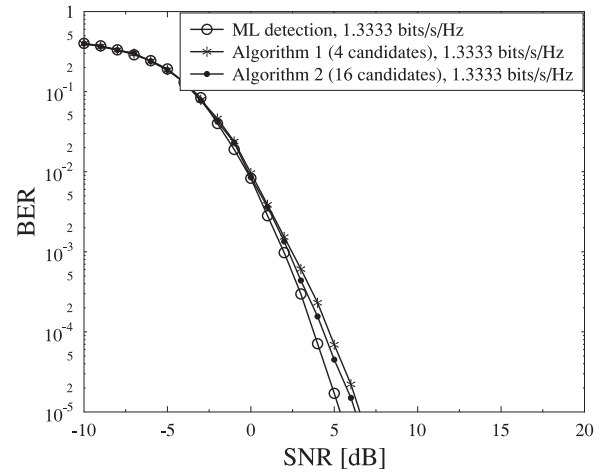


Fig. 9. BER performances of three schemes applying ML detection, reduced-complexity detection Algorithm 1 with 4 candidates, and reduced-complexity detection Algorithm 2 with 16 candidates at the same transmission rate of 1.3333 bits/s/Hz.

complexity in Fig. 7, we can conclude that the detection complexity can be further reduced by limiting the maximum number of candidates at the cost of some performance loss. For example, the averaged complexity of the scheme applying 4 candidates is almost 0.6 times that of ML detector at the cost of about 4.67 dB performance loss. Similarly, the averaged complexity of the scheme with 5 candidates is 0.7 times that of ML detector at the cost of only 2.72 dB loss. Meanwhile, the averaged complexity orders of the proposed reduced-complexity detector 2 using 1 iteration and 16 iterations are compared in Fig. 7. It is obvious in Fig. 7 that the averaged complexity order of the detector 2 exploiting all index combinations is half that of the ML detector as well as that of the detector 1 employing 16 candidates at the cost of only 2.92 dB performance loss than ML detection.

In order to further illustrate the BER performance vs complexity trade-off of the different schemes shown in Figs. 5 and 6, Fig. 8 shows the SNR required and the average complexity order required for attaining a BER of  $10^{-5}$  for the CS-aided OFDM-STSK-IM system employing decoding Algorithm 1. As shown in Fig. 8, employing more candidates results in a reduced SNR required for attaining a BER of  $10^{-5}$ . Furthermore, no performance improvement is attained employing beyond more than 9 candidates. Fig. 8 also shows the average complexity order of the decoder when employing different number of candidates. It becomes clear that using more candidates results in a higher complexity order. According to Figs. 6 and 8, Algorithm 2 applying 16 candidates has a similar performance to that of Algorithm 1 applying 5 candidates, but Algorithm 2 has a lower average complexity order. As a result, for the proposed CS-aided OFDM-STSK-IM scheme employing reduced-complexity detectors, we can strike a flexible performance vs detection complexity trade-off by appropriately adjusting the maximum number of candidates exploited. Finally, the choice of employing Algorithm 1 or Algorithm 2 also depends on the performance vs complexity trade-off.

In Figs. 9 and 10 higher transmission rates are investigated. The schemes in Fig. 9 use  $K = 2$  active indices out of  $N_a =$

TABLE III  
 AVERAGED COMPLEXITY ORDERS FOR THREE SCHEMES APPLYING THREE CONFIGURATIONS

Transmission Rate	ML Detector	Algorithm 1					Algorithm 2	
		1 Candidate	2 Candidates	3 Candidates	4 Candidates	16 Candidates	1 Candidate	16 Candidates
1.1111 bits/s/Hz	$\mathcal{O}(1024)$	$\mathcal{O}(166.924)$	$\mathcal{O}(316.353)$	$\mathcal{O}(431.835)$	$\mathcal{O}(611.657)$	$\mathcal{O}(1024)$	$\mathcal{O}(83.5232)$	$\mathcal{O}(512)$
1.3333 bits/s/Hz	$\mathcal{O}(4096)$	$\mathcal{O}(731.2384)$	$\mathcal{O}(1379.98)$	$\mathcal{O}(1760.956)$	$\mathcal{O}(2577.016)$	$\mathcal{O}(4096)$	$\mathcal{O}(181.1584)$	$\mathcal{O}(1024)$
2 bits/s/Hz	$\mathcal{O}(262144)$	$\mathcal{O}(42732.524)$	$\mathcal{O}(80986.638)$	$\mathcal{O}(110549.627)$	$\mathcal{O}(156583.992)$	$\mathcal{O}(262144)$	$\mathcal{O}(2672.7724)$	$\mathcal{O}(16384)$

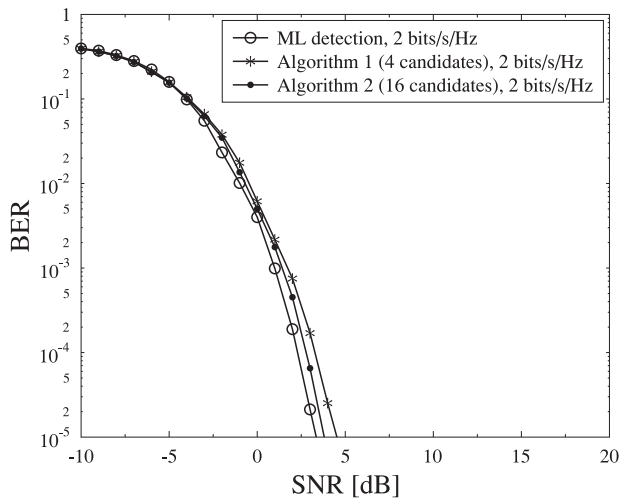


Fig. 10. BER performances of three schemes applying ML detection, reduced-complexity detection Algorithm 1 with 4 candidates, and reduced-complexity detection Algorithm 2 with 16 candidates at the same transmission rate of 2 bits/s/Hz.

16 available indices in each group of the virtual domain,  $M_g = 8$  subcarriers in each group of the frequency domain and the STSK scheme is specified by  $(2, 2, 2, 2, 4)$ . The transmission rate is 1.3333 bits/s/Hz. The performance of the ML detector, of the reduced-complexity Algorithm 1 applying 4 candidates and the reduced-complexity Algorithm 2 applying 16 candidates are compared in Fig. 9. It is shown in Fig. 9 that the performance of Algorithm 2 applying 16 candidates is about 0.25 dB and 1 dB lower than that of Algorithm 1 and that of the ML detector, respectively. More quantitatively, Algorithm 1 has 0.75 dB performance loss compared to the ML detector at a BER value of  $10^{-5}$ . We conclude that using 4 candidates in Algorithm 1 is sufficient for the system in Fig. 9 to attain a better performance, despite having a lower decoding complexity. Additionally, in order to further reduce the complexity, Algorithm 2 applying 16 candidates can be invoked by the proposed system for striking a performance vs complexity trade-off. Similarly, the system of Fig. 10 activates  $K = 4$  indices out of  $N_a = 16$  available indices in each group in the virtual domain and the STSK  $(4, 2, 4, 2, 2)$  encoder is also applied, which has a transmission rate of 2 bits/s/Hz. It is shown in Fig. 10 that Algorithm 1 applying 4 candidates achieves about 1 dB lower performance than the ML detector. Algorithm 2 applying 16 candidates has only 0.5 dB lower performance compared to that of the ML detector. In conclusion, similar trends are valid for both Figs. 9 and 10.

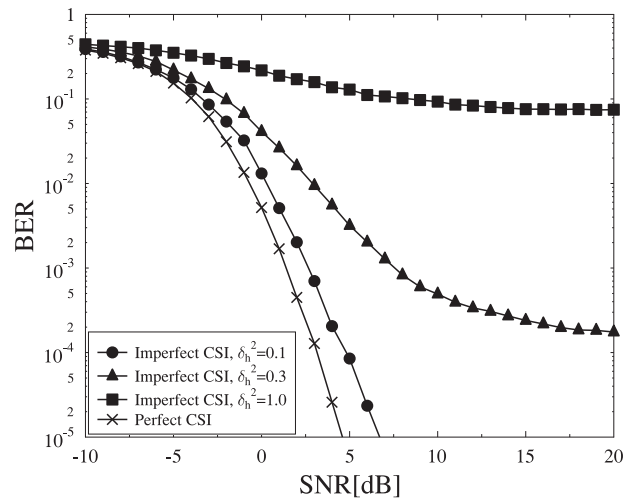


Fig. 11. BER performances of the proposed CS-aided OFDM-STSK-IM system applying ML detection under the imperfect CSI at the transmission rate of 1.1111 bits/s/Hz.

Furthermore, the averaged complexity orders for ML detection, the reduced-complexity Algorithm 1 and Algorithm 2 applying the three transmission rates of 1.1111, 1.3333 and 2 bits/s/Hz are compared in Table III, where the same conclusions reported for Fig. 8 apply.

In Fig. 11, we present simulation results for the proposed CS-aided system under both perfect and imperfect CSI at the transmission rate of 1.1111 bits/s/Hz in order to characterize the effects of imperfect channel estimation on the BER performance. At the receiver, the error of channel estimation is assumed to be complex Gaussian distributed with a mean of zero and a variance of  $\delta_h^2$  [47]. In Fig. 11, we show the resultant BER performances for  $\delta_h^2 = 0.1, 0.3$  and  $1.0$ . Compared to the proposed system under perfect CSI, the system relying on realistic imperfect channel estimation shows an evident performance loss. Additionally, it is shown in Fig. 11 that there is a higher BER performance degradation upon increasing the power of the channel estimation error.

Fig. 12 shows the attainable performance of the 1/2-rate RSC-coded proposed CS-aided OFDM-STSK-IM system of Fig. 4 employing an interleaver depth of 320000 bits, while using a gradually increasing number of inner-outer decoding iterations of 1 to 6. Here, we use the SISO decoder of (23). It is shown in Fig. 12 that there is an evident performance improvement when increasing the number of inner-outer decoding iterations. Additionally, the system attains an infinitesimally low BER at

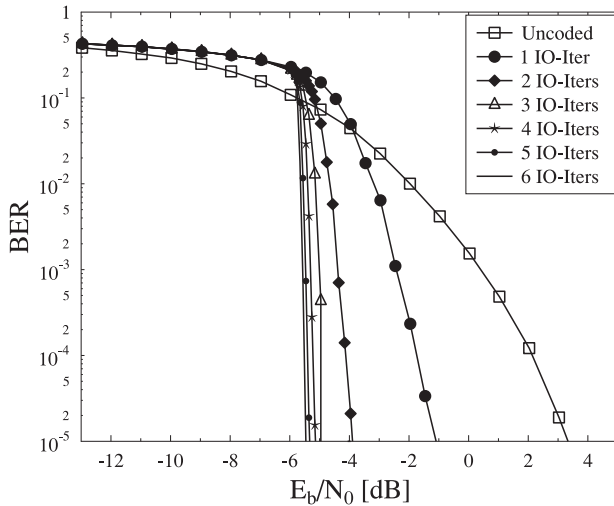


Fig. 12. BER performances of the 1/2-rate, RSC-coded CS-aided OFDM-STSK-IM scheme, while using an interleaver depth of 320 000 bits. 6 inner-outer detection iterations are applied. Here, IO-Iter is the abbreviation of inner-outer iteration.

around  $E_b/N_0 = -5.5$  dB when using 6 inner-outer decoding iterations.

#### IV. CONCLUSION

In this paper, we proposed a novel space-time frequency index modulation scheme relying on CS-aided reduced-complexity detections for transmission over frequency-selective channels. The information bits are transmitted using space, time and frequency dimensions to improve the spectral efficiency as well as the BER performance. In our simulation, the proposed CS-aided OFDM-STSK-IM system employing the ML detector has the best BER performance, as seen in Fig. 5. Quantitatively, it has a 7.92 dB better performance than the classical OFDM-STSK system at the complexity order of  $\mathcal{O}(1024)$ . Then, in order to reduce the high complexity of the ML detector, a pair of reduced-complexity detectors were also proposed in the paper. However, we can keep the lower complexity by adjusting the maximum number of candidates employed in the system at the cost of some performance loss. In addition, the choice of these two reduced-complexity detectors depends on the preference of the complexity or the performance of the proposed system. In order to achieve a near-capacity performance, a 1/2-rate RSC code was applied to the proposed scheme and iterative decoding between the CS-aided OFDM-STSK-IM soft decoder and RSC decoder was employed. It is shown in Fig. 12 that the system attains an infinitesimally low BER at around  $E_b/N_0 = -5.5$  dB of using 6 inner-outer decoding iterations. However, the efficient design of the CS technique's measurement matrix is one of the most challenging issues of the proposed system and the decoding complexity order is increased, when we increase the size of the virtual domain  $N_a$ . Therefore, our future work will include tackling these two challenges. Additionally, the proposed CS-aided OFDM-STSK-IM system can be applied in a downlink scenario where multiple-users are supported at an improved data rate and BER performance.

#### REFERENCES

- [1] S. Sugiura, S. Chen, and L. Hanzo, "Coherent and differential space-time shift keying: A dispersion matrix approach," *IEEE Trans. Commun.*, vol. 58, no. 11, pp. 3219–3230, Nov. 2010.
- [2] M. I. Kadir, S. Sugiura, S. Chen, and L. Hanzo, "Unified MIMO-multicarrier designs: A space-time shift keying approach," *IEEE Commun. Surveys Tuts.*, vol. 17, no. 2, pp. 550–579, Nov. 2015.
- [3] R. Y. Mesleh, H. Haas, S. Sinanovic, C. W. Ahn, and S. Yun, "Spatial modulation," *IEEE Trans. Veh. Technol.*, vol. 57, no. 4, pp. 2228–2241, Jul. 2008.
- [4] J. Li, M. Wen, X. Cheng, Y. Yan, S. Song, and M. H. Lee, "Generalized precoding-aided quadrature spatial modulation," *IEEE Trans. Veh. Technol.*, vol. 66, no. 2, pp. 1881–1886, Feb. 2017.
- [5] J. Jeganathan, A. Ghayeb, L. Szczecinski, and A. Ceron, "Space shift keying modulation for MIMO channels," *IEEE Trans. Wireless Commun.*, vol. 8, no. 7, pp. 3692–3703, Jul. 2009.
- [6] M. Driusso, F. Babich, M. I. Kadir, and L. Hanzo, "OFDM aided space-time shift keying for dispersive downlink channels," in *Proc. IEEE Veh. Technol. Conf.*, Sep. 2012, pp. 1–5.
- [7] M. I. Kadir, S. Chen, K. Hari, K. Giridhar, and L. Hanzo, "OFDM-aided differential space-time shift keying using iterative soft multiple-symbol differential sphere decoding," *IEEE Trans. Veh. Technol.*, vol. 63, no. 8, pp. 4102–4108, Oct. 2014.
- [8] I. A. Hemadeh, M. El-Hajjar, S. Won, and L. Hanzo, "Layered multi-group steered space-time shift-keying for millimeter-wave communications," *IEEE Access*, vol. 4, pp. 3708–3718, 2016.
- [9] I. A. Hemadeh, M. El-Hajjar, S. Won, and L. Hanzo, "Multi-set space-time shift keying and space-frequency space-time shift keying for millimeter-wave communications," *IEEE Access*, vol. 5, pp. 8324–8342, 2016.
- [10] I. A. Hemadeh, M. El-Hajjar, S. Won, and L. Hanzo, "Multiuser steered multiset space-time shift keying for millimeter-wave communications," *IEEE Trans. Veh. Technol.*, vol. 66, no. 6, pp. 5491–5495, Jun. 2017.
- [11] E. Basar, "Index modulation techniques for 5G wireless networks," *IEEE Commun. Mag.*, vol. 54, no. 7, pp. 168–175, Jul. 2016.
- [12] N. Ishikawa, S. Sugiura, and L. Hanzo, "Subcarrier-index modulation aided OFDM—Will it work?" *IEEE Access*, vol. 4, pp. 2580–2593, 2016.
- [13] B. Shamasundar, S. Jacob, S. Bhat, and A. Chockalingam, "Multidimensional index modulation in wireless communications," unpublished paper, 2017. [Online]. Available: <http://arxiv.org/abs/1702.03250>
- [14] T. Datta, H. S. Eshwaraiah, and A. Chockalingam, "Generalized space-and-frequency index modulation," *IEEE Trans. Veh. Technol.*, vol. 65, no. 7, pp. 4911–4924, Jul. 2016.
- [15] E. Basar, U. Aygolu, E. Panayirci, and H. V. Poor, "Orthogonal frequency division multiplexing with index modulation," *IEEE Trans. Signal Process.*, vol. 61, no. 22, pp. 5536–5549, Nov. 2013.
- [16] P. Yang, M. D. Renzo, Y. Xiao, S. Li, and L. Hanzo, "Design guidelines for spatial modulation," *IEEE Commun. Surveys Tuts.*, vol. 17, no. 1, pp. 6–26, First Quarter 2015.
- [17] R. Fan, Y. J. Yu, and Y. L. Guan, "Generalization of orthogonal frequency division multiplexing with index modulation," *IEEE Trans. Wireless Commun.*, vol. 14, no. 10, pp. 5350–5359, Oct. 2015.
- [18] M. Wen, E. Basar, Q. Li, B. Zheng, and M. Zhang, "Multiple-mode orthogonal frequency division multiplexing with index modulation," *IEEE Trans. Commun.*, vol. 65, no. 9, pp. 3892–3906, Sep. 2017.
- [19] Y. Xiao, S. Wang, L. Dan, X. Lei, P. Yang, and W. Xiang, "OFDM with interleaved subcarrier-index modulation," *IEEE Commun. Lett.*, vol. 18, no. 8, pp. 1447–1450, Aug. 2014.
- [20] E. Basar, "OFDM with index modulation using coordinate interleaving," *IEEE Wireless Commun. Lett.*, vol. 4, no. 4, pp. 381–384, Aug. 2015.
- [21] J. Choi, "Coded OFDM-IM with transmit diversity," *IEEE Trans. Commun.*, vol. 65, no. 7, pp. 3164–3171, Jul. 2017.
- [22] M. Wen, B. Ye, E. Basar, Q. Li, and F. Ji, "Enhanced orthogonal frequency division multiplexing with index modulation," *IEEE Trans. Wireless Commun.*, vol. 16, no. 7, pp. 4786–4801, Jul. 2017.
- [23] T. Mao, Q. Wang, and Z. Wang, "Generalized dual-mode index modulation aided OFDM," *IEEE Commun. Lett.*, vol. 21, no. 4, pp. 761–764, Apr. 2017.
- [24] E. Basar, "On multiple-input multiple-output OFDM with index modulation for next generation wireless networks," *IEEE Trans. Signal Process.*, vol. 64, no. 15, pp. 3868–3878, Aug. 2016.
- [25] B. Zheng, M. Wen, E. Basar, and F. Chen, "Multiple-input multiple-output OFDM with index modulation: Low-complexity detector design," *IEEE Trans. Signal Process.*, vol. 65, no. 11, pp. 2758–2772, Jun. 2017.

- [26] E. Basar and I. Altunbas, "Space-time channel modulation," *IEEE Trans. Veh. Technol.*, vol. 66, no. 8, pp. 7609–7614, Aug. 2017.
- [27] T. Datta, H. S. Eshwariah, and A. Chockalingam, "Generalized space-and-frequency index modulation," *IEEE Trans. Veh. Technol.*, vol. 65, no. 7, pp. 4911–4924, Jul. 2016.
- [28] D. L. Donoho, "Compressed sensing," *IEEE Trans. Inf. Theory*, vol. 52, no. 4, pp. 1289–1306, Apr. 2006.
- [29] Z. Han, H. Li, and W. Yin, *Compressive Sensing for Wireless Networks*. Cambridge, U.K.: Cambridge Univ. Press, 2013. [Online]. Available: <https://books.google.co.uk/books?id=h7g29nWN8z8C>
- [30] Y. Eldar and G. Kutyniok, *Compressed Sensing: Theory and Applications* (ser. Compressed Sensing: Theory and Applications). Cambridge, U.K.: Cambridge Univ. Press, 2012. [Online]. Available: <https://books.google.co.uk/books?id=Gm3ihcJwN0YC>
- [31] E. J. Candes and M. B. Wakin, "An introduction to compressive sampling," *IEEE Signal Process. Mag.*, vol. 25, no. 2, pp. 21–30, Mar. 2008.
- [32] H. Zhang, L. L. Yang, and L. Hanzo, "Compressed sensing improves the performance of subcarrier index-modulation-assisted OFDM," *IEEE Access*, vol. 4, pp. 7859–7873, 2016.
- [33] J. W. Choi, B. Shim, Y. Ding, B. Rao, and D. I. Kim, "Compressed sensing for wireless communications: Useful tips and tricks," *IEEE Commun. Surveys Tuts.*, vol. 19, no. 3, pp. 1527–1550, Third Quarter 2017.
- [34] Z. Gao, L. Dai, C. Qi, C. Yuen, and Z. Wang, "Near-optimal signal detector based on structured compressive sensing for massive SM-MIMO," *IEEE Trans. Veh. Technol.*, vol. 66, no. 2, pp. 1860–1865, Feb. 2017.
- [35] C. E. Shannon, "A mathematical theory of communication," *Bell Syst. Tech. J.*, vol. 27, pp. 623–656, Oct. 1948.
- [36] R. W. Hamming, "Error detecting and error correcting codes," *Bell Syst. Tech. J.*, vol. 29, pp. 41–56, 1950.
- [37] P. Elias, "Coding for noisy channels," *IRE Convention Rep.*, pp. 37–47, 1955.
- [38] C. Berrou and A. Glavieux, "Near optimum error correcting coding and decoding: Turbo-codes," *IEEE Trans. Commun.*, vol. 44, no. 10, pp. 1261–1271, Oct. 1996.
- [39] L. Hanzo, T. H. Liew, B. L. Yeap, R. Y. S. Tee, and S. X. Ng, *Turbo Coding, Turbo Equalisation and Space-Time Coding: EXIT-Chart-Aided Near-Capacity Designs for Wireless Channels*. New York, NY, USA: Wiley-IEEE Press, 2011.
- [40] L. Bahl, J. Cocke, F. Jelinek, and J. Raviv, "Optimal decoding of linear codes for minimizing symbol error rate," *IEEE Trans. Inform. Theory*, vol. 20, no. 2, pp. 284–287, Mar. 1974.
- [41] G. Forney, *Concatenated Codes*. Cambridge, MA, USA: MIT Press, 1966.
- [42] S. Benedetto and G. Montorsi, "Serial concatenation of block and convolutional codes," *Electron. Lett.*, vol. 32, no. 10, pp. 887–888, May 1996.
- [43] J. A. Tropp and A. C. Gilbert, "Signal recovery from random measurements via orthogonal matching pursuit," *IEEE Trans. Inf. Theory*, vol. 53, no. 12, pp. 4655–4666, Dec. 2007.
- [44] M. El-Hajjar and L. Hanzo, "EXIT charts for system design and analysis," *IEEE Commun. Surveys Tuts.*, vol. 16, no. 1, pp. 127–153, May 2014.
- [45] J. Hagenauer, E. Offer, and L. Papke, "Iterative decoding of binary block and convolutional codes," *IEEE Trans. Inf. Theory*, vol. 42, no. 2, pp. 429–445, Mar. 1996.
- [46] P. Robertson, E. Villebrun, and P. Hoeher, "A comparison of optimal and sub-optimal MAP decoding algorithms operating in the log domain," in *Proc. IEEE Int. Conf. Commun.*, Jun. 1995, vol. 2, pp. 1009–1013.
- [47] P. Aquilina and T. Ratnarajah, "Performance analysis of IA techniques in the MIMO IBC with imperfect CSI," *IEEE Trans. Commun.*, vol. 63, no. 4, pp. 1259–1270, Apr. 2015.



**Siyao Lu** received the B.Eng. degree in electronic information science and technology from the Dalian Maritime University, Dalian, China, and the M.Sc. degree from the University of Southampton, Southampton, U.K., where she is currently working toward the Ph.D. degree with the Southampton Wireless Group under the supervision of Prof. L. Hanzo and Dr. M. El-Hajjar. Her research interests mainly include multifunctional multiple input multiple output, index modulation, and millimeter-wave communications.



**Ibrahim A. Hemadeh** received the B.Eng. degree (with first class honor) in computer and communications engineering from the Islamic University of Lebanon, Khalde, Lebanon, in 2010, and the M.Sc. degree in wireless communications (with distinction) and the Ph.D. degree in electronics and electrical engineering from the University of Southampton Southampton, U.K., in 2012 and 2017, respectively. In 2017, he was a Postdoctoral Researcher with the Southampton Wireless Group, University of Southampton. In March 2018, he joined the University of Surrey, Guildford, U.K. His research interests include millimeter-wave communications, multifunctional multiple input multiple output (MIMO), multidimensional (time, space, and frequency) transceiver designs, channel coding, and multiuser MIMO.



**Mohammed El-Hajjar** received the Ph.D. degree in wireless communications from the University of Southampton, Southampton, U.K., in 2008. Following the Ph.D., he joined Imagination Technologies as a design engineer, where he worked on designing and developing Imagination's multi-standard communications platform, which resulted in three patents. He is an Associate Professor with the department of Electronics and Computer Science, University of Southampton. He is the recipient of several academic awards and has published a Wiley-IEEE book and in excess of 80 journal and conference papers. His research interests include the design of intelligent and energy-efficient transceivers, cross-layer optimization for large-scale networks, multiple input multiple output, millimeter wave communications, and radio-over-fiber network design.



**Lajos Hanzo** received the Master's degree in electronics in 1976 and the doctorate degree in 1983. In 2009, he was awarded the honorary doctorate "Doctor Honoris Causa" by the Technical University of Budapest, Budapest, Hungary, and in 2015 by the University of Edinburgh, Edinburgh, U.K. During his 40-year career in telecommunications, he has held various research and academic posts in Hungary, Germany, and the U.K. Since 1986, he has been with the School of Electronics and Computer Science, University of Southampton, Southampton, U.K., where he holds the Chair in telecommunications. He has successfully supervised about 112 Ph.D. students, coauthored 18 John Wiley/IEEE Press books on mobile radio communications totalling in excess of 10 000 pages, published 1700+ research entries at IEEE Xplore, acted both as TPC and General Chair of IEEE conferences, presented keynote lectures, and has been awarded a number of distinctions. He is currently directing a 40-strong academic research team, working on a range of research projects in the field of wireless multimedia communications sponsored by industry, the Engineering and Physical Sciences Research Council, U.K., the European Research Council's Advanced Fellow Grant, and the Royal Society's Wolfson Research Merit Award. He is an enthusiastic supporter of industrial and academic liaison, and he offers a range of industrial courses. He is a Fellow of the Royal Academy of Engineering, the Institution of Engineering and Technology, and the European Association for Signal Processing.